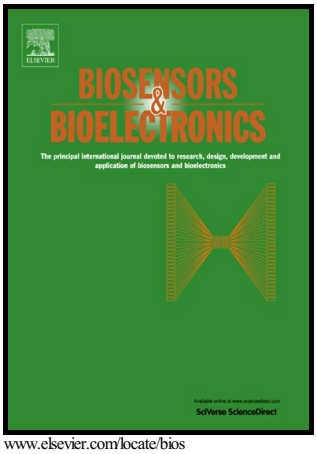

www.elsevier.com/locate/bios

Electrochemically mediated *in situ* growth of electroactive polymers for highly sensitive detection of double-stranded DNA without sequence-preference

Qiong Hu, Qiangwei Wang, Jinming Kong, Lianzhi Li, Xueji Zhang

PII: S0956-5663(17)30653-X
DOI: https://doi.org/10.1016/j.bios.2017.09.045
Reference: BIOS10019

To appear in: *Biosensors and Bioelectronic*

Received date: 21 July 2017
Revised date: 10 September 2017
Accepted date: 25 September 2017

Cite this article as: Qiong Hu, Qiangwei Wang, Jinming Kong, Lianzhi Li and Xueji Zhang, Electrochemically mediated *in situ* growth of electroactive polymers for highly sensitive detection of double-stranded DNA without sequence-preference, *Biosensors and Bioelectronic,* https://doi.org/10.1016/j.bios.2017.09.045

Electrochemically mediated *in situ* growth of electroactive polymers for highly sensitive detection of double-stranded DNA without sequence-preference

Qiong Hu[a,‖], Qiangwei Wang[a,‖], Jinming Kong[a,*], Lianzhi Li[b], Xueji Zhang[c,*]

[a] *School of Environmental and Biological Engineering, Nanjing University of Science and Technology, Nanjing 210094, P. R. China. Email: j.kong@njust.edu.cn. Tel: +86-25-84303109.*

[b] *School of Chemistry and Chemical Engineering, Liaocheng University, Liaocheng 252000, P. R. China.*

[c] *Chemistry Department, College of Arts and Sciences, University of South Florida, East Fowler Ave, Tampa, Florida 33620-4202, United States. Email: xueji@usf.edu.*

[‖] These authors contributed equally to this work.

Corresponding authors: Jinming Kong, Xueji Zhang

Abstract

The ability to directly detect double-stranded DNA (dsDNA) without sequence-preference continues to be a major challenge. Herein, we report an electrochemical method for the direct, highly sensitive detection of dsDNA based on the strand replacement of dsDNA by peptide nucleic acid (PNA) and the *in situ* growth of electroactive polymers through the surface-initiated electrochemically mediated atom transfer radical polymerization (SI-eATRP). Thiolated PNA molecules are firstly self-assembled onto gold electrode surface for the specific recognition of target dsDNA (dsDNA-T), which in turn leads to the formation of a high density of PNA/DNA heteroduplexes on the electrode surface for the subsequent attachment of ATRP initiators *via* the phosphate-Zr^{4+}-carboxylate chemistry. By applying a negative potential to the electrode, the air-stable Cu^{II} deactivators can be reduced into the Cu^{I} activators so as to trigger the surface-initiated polymerization for the *in situ* growth of electroactive polymers. Due to the strand replacement of dsDNA by PNA, dsDNA can be directly detected without sequence-preference. Besides, the growth of polymers enables the modification of numerous electroactive probes, thereby greatly improving the electrochemical signal. Under optimal conditions, a good linearity between the electrochemical signal and the logarithm of dsDNA-T concentration over the range from 1.0 fM to 1.0 nM, with a detection limit of 0.47 fM, can be obtained. Results indicate that it is highly selective, and holds high anti-interference capability in the presence of human serum samples. Therefore, this method offers great promises in providing a universal and efficient solution for the direct detection of dsDNA.

Keywords: electrochemical DNA biosensor; peptide nucleic acid; atom transfer radical polymerization; double-stranded DNA; circulating tumor DNA; liquid biopsy

1. Introduction

Circulating tumor DNAs (ctDNAs) are the tumor-derived fragmented double-stranded DNAs (dsDNAs) that freely circulate in the bloodstream (Alix-Panabières et al., 2012; Diaz Jr and Bardelli, 2014). Considering that the abnormal levels of ctDNAs are indicative of tumor burden and malignant progression (Leon et al., 1977; Schwarzenbach et al., 2011), they can be used as noninvasive biomarkers for the diagnosis and real-time monitoring of tumors based on liquid biopsy (Alix-Panabières et al., 2012; Diaz Jr and Bardelli, 2014). In particular, they are very useful in situations where frequently sampling based on tissue biopsy is too invasive, or if there is insufficient sample available for genotyping (Bellassai and Spoto, 2016). Although a higher level of ctDNAs can often be found in the peripheral blood of tumor patients than do healthy individuals (Leon et al., 1977), the targeted detection of specific ctDNA is a longstanding challenge as a result of the extremely low abundance of ctDNAs in blood (Bellassai and Spoto, 2016; Diehl et al., 2008) and the presence of a high level of other cell-free DNAs (cfDNAs) (Diehl et al., 2008). For the detection of ctDNAs to be clinically meaningful, the prerequisite is to directly detect ctDNAs in their native form (i.e., in the form of dsDNA) with high sensitivity and selectivity, from the viewpoint of technology.

Unlike that of single-stranded DNA (ssDNA) or RNA, which can be specifically recognized by the complementary probes *via* Watson-Crick base pairing, dsDNA–the native form of DNA structure in most cases–lacks such a simple and universal recognition principle (Demidov, 2001). This poses a major challenge on the direct detection of dsDNA. Recently, several approaches have been proposed in this direction. Most of these involve the use of triplex-forming oligonucleotides (TFOs) (Li et al., 2015; Miao et al., 2014; Patterson et al., 2010; Xiao et al., 2013). Notwithstanding the value of the TFOs-based approach in some applications (Ito et al., 1992; Strobel and Dervan, 1991), it is essentially restricted to the use of homopyrimidine/homopurine oligonucleotides that can specifically bind to the major groove of homopyrimidine-homopurine dsDNAs through Hoogsteen and Watson-Crick base pairing (Betts et al., 1995; Patterson et al., 2010; Thuong and Hélène, 1993), which is not practical enough due to the high sequence-preference. Besides, multivalent cations (e.g., Mg^{2+}) and polyamines are required to neutralize the electrostatic repulsion between the negatively-charged TFOs and dsDNAs so as to stabilize the triplexes (Ling et al., 2004). Although the recognition of mixed-base dsDNAs by complementary probes can be facilitated by RecA protein or its fragment (Ferrin and Camerini-Otero, 1991; Voloshin et al.,

1996), the fidelity of RecA-assisted recognition is much lower when compared with that of the "pure" DNA-DNA or DNA-RNA interactions, being tolerant to up to four mismatches (Malkov et al., 1997). Peptide nucleic acid (PNA) is a synthetic DNA analog in which the negatively-charged deoxyribose phosphate backbone of DNA is substituted with a neutral pseudopeptide chain (Nielsen et al., 1991; Ozkan et al., 2002). Relative to ssDNA or RNA, PNA can bind to its complementary target with higher specificity (Egholm et al., 1993; Giesen et al., 1998). More importantly, at low ionic strength, it has the capacity to invade a DNA/DNA duplex in a highly sequence-specific manner (Boffa et al., 1995; Smolina et al., 2005). This is because that the hydrogen bonds at the end of DNA/DNA duplex are weaker than those located internally (Frank-Kamenetskii, 1987; Nonin et al., 1995), while the binding affinity of PNA to the complementary target is much higher than that of the ssDNA (Liu et al., 2006). Thus, PNA has long been served as a duplex invader in biological applications, e.g., fluorescence imaging for *in situ* hybridization assays and transcription regulation (Nielsen, 2010; Pellestor et al., 2008). Mediated by the end invasion of PNA toward dsDNA, Stadler et al. have demonstrated a strategy for the targeted assembly of nanoparticles along dsDNA (Stadler et al., 2011). Pioneering work on the use of strand replacement of dsDNA by PNA through end invasion for the site-specific and sequence-unbiased manipulation and detection of dsDNA was reported by Smolina and co-authors (Smolina et al., 2005). Similarly, Lee et al. reported a direct dsDNA detection method based on the strand replacement of dsDNA by PNA and the preferential binding of graphene oxide (GO) to PNA over DNA/PNA duplex (Lee et al., 2014). Taking advantage of the strand replacement of dsDNA by PNA, dsDNA can be directly detected without sequence-preference, which is of vital importance to practical applications.

Inspired by these previous work, herein, we report a highly sensitive electrochemical method for the direct detection of dsDNA based on the strand replacement of dsDNA by PNA and the *in situ* growth of electroactive polymers through the surface-initiated electrochemically mediated atom transfer radical polymerization (SI-eATRP). The scheme of the electrochemical detection of dsDNA is illustrated in Scheme 1. Briefly, thiolated PNAs are firstly self-assembled onto gold electrode surface and used as the probes for the specific recognition of target dsDNA (dsDNA-T). The interactions of dsDNA-T with the PNA monolayer leads to the binding of PNA to the end of its complementary strand in the dsDNA-T through end invasion and the subsequent replacement of the other strand totally by PNA. Thus, the capture of dsDNA-T can bring a high density of phosphate groups on the electrode surface for the subsequent attachment of ATRP initiators, α-bromophenylacetic acid (BPAA), in the presence of Zr^{4+} ions as the "molecular glues". By applying a negative potential to the gold electrode, the air-stable Cu^{II}

deactivators in the close proximity of electrode surface can be reduced into the Cu^{I} activators electrochemically so as to trigger the surface-initiated polymerization for the *in situ* growth of electroactive polymers, with ferrocenylmethyl methacrylate (FMMA) as the monomer. Compared with the TFOs-based approach, which are essentially restricted to the use of homopyrimidine/homopurine oligonucleotides, our method is applicable to the direct detection of mixed-base dsDNA. In other words, it has no specific restriction on the oligonucleotide sequences (i.e., without sequence-preference), which can be ascribed to the strand replacement of dsDNA by PNA. In addition, growth of long polymeric chains leads to the modification of numerous electroactive probes, thereby greatly improving the electrochemical signal. Since the concentration of the Cu^{I} activator can be readily controlled by the applied potential (E_{app}), the SI-eATRP, which is highly efficient and cost-effective, provides sufficient simplicity in controlling the degree of signal amplification. Under optimal conditions, the resulting electrochemical signal increases linearly along with dsDNA-T concentration over 7 orders of magnitude from 1.0 fM to 1.0 nM, while a signal-on method like this is believed to be highly immune to false-positive results. Results demonstrate that it has high selectivity for dsDNA detection, and holds high anti-interference capability in the presence of complex human serum samples. Therefore, the combined use of PNA as the capture probe and the electrochemically mediated polymerization as a signal amplification strategy offers great promises in providing a highly efficient and sensitive solution for the direct detection of dsDNA.

(Scheme 1 is around here)

2. Material and methods

2.1. Materials and reagents

Thiolated PNA was custom-made by Panagene Inc. (Daejon, Korea). ssDNAs were synthesized and purified by Sangon Biotech (Shanghai) Co., Ltd. (Shanghai, China). The dsDNAs, including target dsDNA (dsDNA-T), one base pair replaced dsDNA (dsDNA-1), three base pairs replaced dsDNA (dsDNA-3) and control dsDNA (dsDNA-C), were prepared, respectively, by heating the mixture of equimolar complementary ssDNAs at 95 °C with A300 Fast Thermal Cycler (LongGene, Hangzhou, China) for 15 min, and then by annealing gradually to form the duplexes. The sequences of PNA and dsDNAs are shown in Table 1.

(Table 1 is around here)

6-Mercapto-1-hexanol (MCH), bathophenanthrolinedisulfonic acid disodium salt hydrate (BPDS), and ferrocenylmethyl methacrylate (FMMA) were purchased from Sigma-Aldrich (Shanghai) Trading

Co., Ltd. (Shanghai, China). *α*-Bromophenylacetic acid (BPAA), copper(II) bromide ($CuBr_2$), zirconium dichloride oxide octahydrate ($ZrOCl_2 \cdot 8H_2O$), potassium hexafluorophosphate (KPF_6), potassium bromide (KBr), and lithium perchlorate trihydrate ($LiClO_4 \cdot 3H_2O$) were purchased from J&K Scientific Ltd. (Shanghai, China). Normal human serum was obtained from Shanghai YiJi Industrial Co., Ltd. (Shanghai, China). *N*,*N*-Dimethylformamide (DMF) and other reagents were all purchased from Sinopharm Chemical Reagent Co., Ltd. (Shanghai, China). All chemicals were of at least analytical pure and used as supplied. Ultrapure water (≥ 18.25 MΩ) was used as the water source throughout the work.

0.1 M NaH_2PO_4/Na_2HPO_4 (PBS, pH 7.4) was used as the stocking/washing buffer for ssDNAs and dsDNAs. dsDNA samples at different concentrations were prepared by serially diluting the stocking solution with 0.1 M PBS. 10 mM Cu^{II} deactivator was prepared by dissolving $CuBr_2$ and BPDS, in a stoichiometric ratio of 1:2, into ultrapure water. The eATRP solution (pH 7.0) was freshly prepared by successively adding 0.9 mL of DMF, 50 μL of 10 mM FMMA (dissolved in DMF), 50 μL of 10 mM Cu^{II} deactivator, 0.5 mL of 1.0 M KBr, and 3.5 mL of 0.1 M KPF_6 into the electrochemical cell; the final concentrations of FMMA and Cu^{II} deactivator were both at 0.1 mM.

2.2. Apparatus

All electrochemical experiments were carried out at room temperature, using a modified gold electrode (Φ = 2.0 mm) as the working electrode, a platinum wire as the auxiliary electrode, and a saturated calomel electrode (SCE) as the reference electrode, respectively. A RST5200F electrochemical workstation (Suzhou Risetest Electronic Co. Ltd., China) was used for cyclic voltammetry (CV), square wave voltammetry (SWV) and linear sweep voltammetry (LSV) experiments. Electrochemical impedance spectroscopy (EIS) measurements (frequency range: 100 KHz to 0.1 Hz; open circuit potential: 0.18 V; amplitude of the applied sine wave potential: 5.0 mV) were performed on Autolab/PGSTAT302N (Eco Chemie, Netherlands), in 0.1 M KNO_3 containing 5.0 mM $[Fe(CN)_6]^{3-/4-}$ as the redox probes. Scanning electron microscopy (SEM) image was collected on a Quanta FEG 250 field emission scanning electron microscopy (FEI, USA).

2.3. Electrochemical detection of dsDNA

Prior to use, the gold electrode was pretreated according to our previous work (Hu et al., 2015). Next, PNA probes were immobilized by adding 5.0 μL of 0.5 μM PNA aqueous solution onto the gold electrode, followed by an incubation at 37 °C for 1.5 h. After a wash with ultrapure water, the PNA coated electrode was dipped in 400 μL of 5.0 mM MCH (prepared with 60% ethanol) for 30 min to block the nonspecific binding sites (Hu et al., 2015), and rinsed with ethanol and ultrapure water. Then, 10 μL of dsDNA was pipetted onto the electrode. To increase the hybridization efficiency and thus

largely shorten the hybridization time, the electrode was subjected to a preincubation at 80 °C for 5.0 min before it was incubated at 37 °C for 2.0 h. Followed by a thorough rinse with 0.1 M PBS to remove any nonspecifically adsorbed DNA, the electrode was dipped in 400 μL of 5.0 mM $ZrOCl_2$ (prepared with 10% ethanol) at 37 ^oC for 15 min, and moderately rinsed with 10% ethanol. After a soak in 400 μL of 1.0 mM BPAA (prepared with 15% ethanol) at 37 ^oC for 30 min and a sequential rinse with 15% ethanol and ultrapure water, the electrode was dipped in the eATRP solution for the modification of FMMA *via* the SI-eATRP under a negative potential. Prior to measurement, the electrode was treated with LSV (initial potential: 0 V; final potential: 0.25 V; scan rate: 1.0 V s^{-1}) and rinsed thoroughly with DMF and ultrapure water to remove any physically adsorbed species. Finally, the modified electrode was dipped in 0.5 M $LiClO_4$, and then SWV (initial potential: 0 V; final potential: 0.6 V; increase potential: 4.0 mV s^{-1}; potential amplitude: 25 mV, quiet time: 30 s) was applied to record the electrochemical signal.

3. Results and discussion

3.1. Characterizations

To study the feasibility of the PNA-based direct detection of dsDNA, the strand replacement of dsDNA by PNA was firstly validated by resolving the PNA/DNA heteroduplex and the intact dsDNA (i.e., DNA/DNA homoduplex) using nondenaturing polyacrylamide gel electrophoresis (native-PAGE). Theoretically, due to less negative charge of the PNA/DNA heteroduplex relative to the DNA/DNA homoduplex, it tends to migrate slower in the gel. As shown in Fig. 1A, the incubation of PNA with the solution of dsDNA-T (lane 3) presents a strip as is observed for the PNA/DNA heteroduplex (lane 2), indicative of the strand replacement of dsDNA by PNA. Considering that the hydrogen bonds at the end of dsDNA are weaker than those located internally (Frank-Kamenetskii, 1987; Nonin et al., 1995) and the binding affinity of PNA to the complementary target is much higher than that of to the ssDNA (Liu et al., 2006), the PNA-based direct detection of dsDNA is likely to proceed as follows: the PNA probe firstly bind to the end of its complementary strand in the dsDNA-T through end invasion, followed by the migration of PNA along the complementary strand and the complete replacement of the other strand by PNA (Lee et al., 2014; Smolina et al., 2005). Taking advantage of the strand replacement of dsDNA by PNA, dsDNA can therefore be directly detected without sequence-preference, rendering great potential in practical applications.

(Fig. 1 is around here)

Before we discuss the SI-eATRP, it is necessary to specify the structures of the Cu^I activator and the

Cu^{II} deactivator. In general, the preferred coordination numbers of the closed-shell $3d^{10}$ Cu^{I} center and the open-shell $3d^{9}$ Cu^{II} center in copper-amine complexes are 4 and 5, respectively (Fantin et al., 2015; Hu et al., 2016). As a bidentate ligand, two BPDS molecules are required to fill up the coordination sphere of the Cu^{I} center; for the Cu^{II} center, however, an extra ligand (e.g., anions, solvent molecules) is needed to complete its coordination sphere (Fantin et al., 2015). So, in the presence of BPDS and Br^- as the ligands, the Cu^{I} activator and the Cu^{II} deactivator are in the form of $Cu^{I}/BPDS_2$ and $Cu^{II}Br/BPDS_2$, respectively (Fantin et al., 2015). In the following discussion, the formalisms of Cu^{I}/L and $Cu^{II}Br/L$ (L = BPDS) are adopted for simplicity. Hitherto, BPDS has never been studied as a ligand in the ATRP reactions. To evaluate the possibility of exploiting BPDS as a ligand in the eATRP, the redox properties of the Cu^{I}/Cu^{II} couple and of the $[Cu^{I}/L]/[Cu^{II}Br/L]$ couple were studied with CV. As shown in Fig. S1, the apparent formal potential ($E°'$), as estimated from $E_{1/2} = (E_{ox} + E_{red})/2$ (Fantin et al., 2015; Hu et al., 2016), of the Cu^{I}/Cu^{II} couple is at -0.013 V *vs.* SCE (Fig. S1,b); for the $[Cu^{I}/L]/[Cu^{II}Br/L]$ couple, it negatively shifts to -0.11 V *vs.* SCE (Fig. S1,c). So, the BPDS ligand preferentially stabilizes Cu^{II} over Cu^{I} (Hu et al., 2016; Pintauer et al., 2003). Due to the negative shift of the reduction potential as a result of the preferential stabilization of Cu^{II} over Cu^{I} by the BPDS ligand, the electrochemical reduction of $Cu^{II}Br/L$ into Cu^{I}/L can be realized at a negative potential. Thus, BPDS can be served as an ideal ligand in the eATRP reactions. Further, the relative stability of the Cu^{I}/L and Cu^{II}/L complexes, i.e., the ratio of their stability constants (β^{I}, β^{II}), is calculated from the reduction peak potential, according to Equation 1:

$$E^{\ominus}_{\{[Cu^{I}/L]/[Cu^{II}/L]\}} = E^{\ominus}_{[Cu^{I}/Cu^{II}]} + \frac{RT}{F}\ln\frac{\beta^{I}}{\beta^{II}} \quad (1)$$

where $E^{\ominus}_{\{[Cu^{I}/L]/[Cu^{II}/L]\}}$, $E^{\ominus}_{[Cu^{I}/Cu^{II}]}$, R, and F represent the reduction peak potentials of the $[Cu^{I}/L]/[Cu^{II}/L]$ couple and of the Cu^{I}/Cu^{II} couple, the universal gas constant, and the Faraday constant, respectively. As calculated from the reduction peak potential, β^{II} is about 200 times larger than β^{I}, which is in good agreement with the higher electron-withdrawing character of the Cu^{II} center relative to the Cu^{I} center as a result of the higher charge (Chen et al., 1981; Hu et al., 2017).

By applying a negative potential to the gold electrode, the air-stable $Cu^{II}Br/L$ in the close proximity of electrode surface can be electrochemically reduced into the catalytically active Cu^{I}/L so as to trigger the surface-initiated polymerization for the *in situ* growth of electroactive polymers. Since the SI-eATRP is performed at a constant potential (E_{app}), the $\Delta E = E_{app} - E_{1/2}$ ($E_{1/2}$ corresponds to the half sum of the anodic and cathodic peak potentials of the $[Cu^{I}/L]/[Cu^{II}Br/L]$ couple) can be varied to control the concentration of the Cu^{I} activator, according to the Nernst equation:

$$E_{app} = E_{1/2} + \frac{RT}{nF}\ln\frac{C_{[Cu^{II}Br/L]}}{C_{[Cu^{I}/L]}} \quad (2)$$

Clearly, in the absence of mass transport limitations, the concentration of Cu^{I}/L can be dictated by the E_{app}, rendering a good control over the SI-eATRP. Moreover, the *in situ* generated Cu^{I}/L will enrich at the electrode surface, thereby significantly accelerating the growth of electroactive polymers. Due to the modification of numerous electroactive probes, a great improvement in the electrochemical signal can be achieved. To ascertain the potential window for the accurate control of the SI-eATRP, the cyclic voltammogram of the modified electrode, onto which the ATRP initiators have already been attached *via* the phosphate-Zr^{4+}-carboxylate chemistry, in the FMMA-free eATRP solution was collected. As shown in Fig. S2, the cathodic scan results in a reduction peak at the potential of -0.52 V *vs.* SCE, which is derived from the electrochemical reduction of Cu^{II}Br/L into Cu^{I}/L (Fantin et al., 2015). According to Equation 2, a lower potential can generate a higher concentration of Cu^{I}/L. However, a faster polymerization as a result of a higher concentration of Cu^{I}/L will deteriorate the polymerization control, likely due to the loss of C-Br functional groups (Fantin et al., 2015). Although a higher potential, on the other hand, allows a better control over the polymerization, a largely prolonged polymerization time will be suffered due to the poor catalytic efficiency. For these reasons, the SI-eATRP is performed at the reduction peak potential of the [Cu^{I}/L]/[Cu^{II}Br/L] couple, that is, at -0.52 V *vs.* SCE.

Initial experiments were carried out to verify the feasibility and reliability of exploiting PNA as the capture probe and the electrochemically mediated polymerization as a signal amplification strategy for the direct, highly sensitive detection of dsDNA. As shown in Fig. 1B, no significant oxidation current can be detected when PNA (Fig. 1B,b), dsDNA-T (Fig. 1B,c), Zr^{4+} (Fig. 1B,d), BPAA (Fig. 1B,e), Cu^{II}Br/L (Fig. 1B,f) or FMMA (Fig. 1B,g) was not added during the sequential modification of the electrode, on the other hand, a clear oxidation current at the potential of ~ 0.3 V (*vs.* SCE) can be detected in the case that all the components have been added (Fig. 1B,a). The oxidation current is derived from the electrochemical oxidation of ferrocene into ferrocenium cation, which is in good agreement with the previous reports (Fan et al., 2003; Hu et al., 2015). The observation that the oxidation current can only be clearly detected after adding all the components validates the feasibility and reliability of our method. Moreover, such a high signal-to-noise ratio is essential for the highly sensitive detection of dsDNA, while a "signal-on" method like this is highly immune to false-positive results (Fan et al., 2003). Further, the surface morphology of the electrode obtained after the SI-eATRP was characterized with SEM. As shown in Fig. S3, a high density of mound-like eminences can be discerned after the SI-eATRP, confirming the formation of polymers. After the SI-eATRP, the resulting electrode was also characterized with CV at different scan rates. As can be seen from Fig. 1C, there is a good linearity between the redox currents and the scan rate, which is a typical characteristic of the

diffusion-independent redox processes, indicating that the newly formed electroactive polymers are attached to the electrode surface (Fan et al., 2003; Grabowska et al., 2014; Hu et al., 2015).

The modification of the electrode was characterized with EIS, which is highly sensitive to the changes occurring at electrode surface (Dubuisson et al., 2011). For the Nyquist plot, the semicircle at high frequency region corresponds to the charge-transfer resistance (R_{ct}) (Dubuisson et al., 2011). As expected, the bare electrode shows the smallest R_{ct} (~0.12 kΩ, Fig. 1D,a). The immobilization of PNA probes (~0.49 kΩ, Fig. 1D,b), as well as the blocking of electrode surface with MCH (~0.62 kΩ, Fig. 1D,c), leads to an increase in the R_{ct}; this is due to the steric hindrance arising from the self-assembled monolayer(s) (Hu et al., 2015; Liu et al., 2010). The addition of dsDNA-T results in a further increase in the R_{ct} (~0.95 kΩ, Fig. 1D,d), indicative of the formation of PNA/DNA heteroduplexes (Hu et al., 2015; Noorbakhsh and Salimi, 2011). In the presence of Zr^{4+} ions, the negatively-charged redox probes can be electrostatically adsorbed to the PNA/DNA heteroduplexes, leading to a large increase in the R_{ct} as a result of the blockage from the pre-adsorbed redox probes to the charge transfer (~1.31 kΩ, Fig. 1D,e). Further, the attachment of ATRP initiators is also accompanied by an increase in the R_{ct} (~2.07 kΩ, Fig. 1D,f). Also, a significant increase in the R_{ct} is observed after the SI-eATRP (~9.92 kΩ, Fig. 1D,g), owing to the growth of a high density of highly hydrophobic polymers. These results provide a convincing evidence of the successful modification of the electrode as expected.

3.2. Effects of pH and SI-eATRP time

In the SI-eATRP, the catalytic couple is the Cu^{I}/L and Cu^{II}Br/L complexes, which can be involved in proton transfer reactions (Fantin et al., 2015). So, the pH of the eATRP solution can drastically affect the *in situ* growth of electroactive polymers. Under alkaline conditions, both the activation and deactivation reactions can be seriously retarded as a result of the formation of the Cu^{II}OH/L complex (Fantin et al., 2015); an alkaline pH can therefore significantly lower the catalytic efficiency. However, an acidic solution can protonate the BPDS ligand, lowering its ability to coordinate the Cu^{I} and Cu^{II} centers, leading to a dissociation of Cu^{I}/L and Cu^{II}Br/L, as well as the disproportionation of Cu^{I} (Fantin et al., 2015). With these in mind, the SI-eATRP was carried out at pH 7.0.

The dynamic growth of polymers correlates with the enrichment of ferrocene onto the electrode surface. In other words, longer polymerization time leads to the modification of more ferrocene. To ascertain the optimal time for the SI-eATRP, CV was adopted to monitor the dynamic growth of polymers. As shown in Fig. S4, in the presence of 10 μL of 1.0 nM dsDNA-T, the oxidation current increases obviously with the SI-eATRP time during the first 50 min. Afterwards, no significant increase in oxidation current can be observed, presumably due to the greatly increased steric hindrance along

with the dynamic growth of polymers, as well as the radical termination (Ma et al., 2004; Wu et al., 2014). The fast reaction kinetics indicate that the SI-eATRP is highly efficient. In the following experiments, the SI-eATRP time was set to 60 min.

3.3. Analytical performance

Under optimal conditions, the analytical performance of our method was investigated with varying concentrations of dsDNA-T. As shown in Fig. 2, the oxidation current at the potential of ~0.3 V (*vs.* SCE) increases with the increasing of dsDNA-T concentration. As a result, this is a "signal-on" method, which is believed to be highly immune to false-positive results. Moreover, there is a good linearity between the oxidation current and the logarithm of dsDNA-T concentration over 7 orders of magnitude from 1.0 fM to 1.0 nM, where the regression equation is I (μA) = 18.69 + 1.16 lg [$C_{\text{dsDNA-T}}$/pM] (R^2 = 0.997). The limit of detection (LOD) is calculated to be 0.47 fM ($C_{\text{LOD}} = 3\sigma$/slope), which is much lower than many other methods, as summarized in Table 2. The high sensitivity can be due to the modification of numerous electroactive probes as a result of the *in situ* growth of a high density of electroactive polymers. Therefore, our method can be applied to the highly sensitive detection of dsDNA. The total cost of each test is calculated to be lower than 0.1 $; so, our method is rather cost-effective. In addition, it is operationally simple (without the use of any complex nanomaterials or enzymes) and highly efficient (the turnaround for each test is ~ 6.0 h), thus showing great potential for the direct detection of dsDNA.

(Fig. 2 is around here)

(Table 2 is around here)

3.4. Selectivity

To evaluate the selectivity of our method, the electrochemical responses from three other dsDNAs, including dsDNA-1, dsDNA-3, and dsDNA-C, were compared with that from the dsDNA-T. As shown in Fig. 3A, the electrochemical response from dsDNA-1 and dsDNA-3 is, respectively, as low as 25.1% and 13.2% of that from the dsDNA-T, while no obvious difference relative to the background current can be observed for the dsDNA-C. The observation that even a one base pair difference can lead to a significant decrease of the electrochemical response demonstrates that our method is highly selective for dsDNA-T detection. This can be ascribed to the high specificity of the PNA probe, since the presence of mismatched base(s) is adverse to the formation of PNA/DNA heteroduplexes (Giesen et al., 1998; Smolina et al., 2005), which in turn greatly reduces the number of phosphate groups and consequently the electrochemical response.

(Fig. 3 is around here)

3.5. Reproducibility, stability and anti-interference capability

The reproducibility of our method was evaluated on the basis of the intra- and inter-assays (n = 6). The variation coefficients of the intra-assay and inter-assay with respect to the repeated detection of 1.0 nM dsDNA-T are 4.3% and 4.8%, respectively, indicating that the detection of dsDNA based on our method is highly reproducible.

Further, after the SI-eATRP, the stability of the modified electrode was studied by a storage test in a moisture-saturated environment at 4 °C. We found that, up to 95.8% of the electrochemical response can be retained after a three-week storage. Of note, this value is derived from a comparison of the average value of the electrochemical responses of two sets of identically prepared electrodes; each set consists of six electrodes and one set was measured immediately after preparation while the other was measured after a three-week storage in a moisture-saturated environment at 4 °C. Thus, the modified electrode possesses satisfactory stability.

Also, the anti-interference capability of our method has been studied by a comparison of the electrochemical responses in the presence (Case 1) and absence (Case 2) of 10% normal human serum. As shown in Fig. 3B, the electrochemical response from Case 1 is, respectively, 96.3%, 89.8% and 83.4% of that from Case 2 for 1.0 nM, 1.0 pM and 1.0 fM dsDNA-T. By virtue of its good analytical performance in the presence of 10% serum samples, it can be concluded that our method holds high anti-interference capability, thus showing great potential in practical applications.

4. Conclusions

In summary, we have demonstrated an electrochemical method for the direct, highly sensitive detection of dsDNA based on the strand replacement of dsDNA by PNA and the *in situ* growth of electroactive polymers through the SI-eATRP. Taking advantage of the strand replacement of dsDNA by PNA, dsDNA can be directly detected without sequence-preference, which is superior to the TFOs-based methods and is of vital importance to the detection of dsDNA (e.g., ctDNAs). Due to the modification of numerous electroactive probes as a result of the *in situ* growth of a high density of electroactive polymers, a great improvement in the electrochemical signal can be achieved, which is highly efficient and cost-effective. Results also demonstrate that it has high selectivity for dsDNA detection, and holds high anti-interference capability in the presence of complex human serum samples. Therefore, the combined use of PNA as the capture probe and the electrochemically mediated polymerization as a signal amplification strategy offers great promises in providing a highly efficient and sensitive solution for the direct detection of dsDNA. Moreover, the ability to *in situ* graft electroactive polymers from

substrate surface by potential control together with the simplicity, high efficiency and cost-effectiveness of the SI-eATRP makes it great potential for the high-throughput detection on microelectrode arrays.

Acknowledgments

This work was supported by the National Natural Science Foundation of China [21575066].

References

Alix-Panabières, C., Schwarzenbach, H., Pantel, K., 2012. Annu. Rev. Med. 63, 199–215.

Boffa, L.C., Carpaneto, E.M., Allfrey, V.G., 1995. Proc. Natl. Acad. Sci. USA 92, 1901–1905.

Betts, L., Josey, J.A., Veal, J.M., Jordan, S.R., 1995. Science 270, 1838–1841.

Bellassai, N., Spoto, G., 2016. Anal. Bioanal. Chem. 408, 7255–7264.

Chen, Y.W.D., Santhanam, K.S.V., Bard, A.J., 1981. J. Electrochem. Soc. 128, 1460–1467.

Demidov, V.V., 2001. Expert Rev. Mol. Diagn. 1, 343–351.

Diehl, F., Schmidt, K., Choti, M.A., Romans, K., Goodman, S., Li, M., Thornton, K., Agrawal, N., Sokoll, L., Szabo, S.A., Kinzler, K.W., Vogelstein, B., Diaz Jr, L.A., 2008. Nat. Med. 14, 985–990.

Dubuisson, E., Yang, Z., Loh, K.P., 2011. Anal. Chem. 83, 2452−2460.

Diaz Jr, L.A., Bardelli, A., 2014. J. Clin. Oncol. 32, 579−586.

Egholm, M., Buchardt, O., Christensen, L., Behrens, C., Freier, S.M., Driver, D.A., Berg, R.H., Kim, S.K., Nordén, B., Nielsen, P.E., 1993. Nature 365, 556–568.

Frank-Kamenetskii, M., 1987. Nature 328, 17–18.

Ferrin, L.J., Camerini-Otero, R.D., 1991. Science 254, 1494–1497.

Fan, C., Plaxco, K.W., Heeger, A.J., 2003. Proc. Natl. Acad. Sci. USA 100, 9134–9137.

Fantin, M., Isse, A.A., Gennaro, A., Matyjaszewski, K., 2015. Macromolecules 48, 6862−6875.

Giesen, U., Kleider, W., Berding, C., Geiger, A., Ørum, H., Nielsen, P.E., 1998. Nucleic Acids Res. 26, 5004–5006.

Grabowska, I., Singleton, D.G., Stachyra, A., Góra-Sochacka, A., Sirko, A., Zagórski-Ostoja, W., Radecka, H., Stulz, E., Radecki, J., 2014. Chem. Commun. 50, 4196–4199.

Hu, Q., Deng, X., Yu, X., Kong, J., Zhang, X., 2015. Biosens. Bioelectron. 65, 71–77.

Hu, Q., Zhou, B., Li, F., Kong, J., Zhang, X., 2016. Chem. Asian J. 11, 3040−3045.

Hu, Q., Zhou, B., Dang, P., Li, L., Kong, J., Zhang, X., 2017. Anal. Chim. Acta 950, 170−177.

Ito, T., Smith, C.L., Cantor, C.R., 1992. Proc. Natl. Acad. Sci. USA 89, 495–498.

Leon, S.A., Shapiro, B., Sklaroff, D.M., Yaros, M.J., 1977. Cancer Res. 37, 646−650.

Ling, L.S., Butt, H.J., Berger, R., 2004. J. Am. Chem. Soc. 126, 13992–13997.

Liu, J., Tiefenauer, L., Tian, S., Nielsen, P.E., Knoll, W., 2006. Anal. Chem. 78, 470–476.

Liu, X., Qu, X., Fan, H., Ai, S., Han, R., 2010. Electrochim. Acta 55, 6491−6495.

Lee, J., Park, I.S., Jung, E., Lee, Y., Min, D.H., 2014. Biosens. Bioelectron. 62, 140–144.

Li, Z., Miao, X., Xing, K., Zhu, A., Ling, L., 2015. Biosens. Bioelectron. 74, 687–690.

Li, R., Zou, L., Luo, Y., Zhang, M., Ling, L., 2017. Sci. Rep. 7: 44212.

Malkov, V.A., Sastry, L., Camerini-Otero, R.D., 1997. J. Mol. Biol. 271, 168–177.

Ma, H., Hyun, J., Stiller, P., Chilkoti, A., 2004. Adv. Mater. 16, 338–341.

Miao, X., Guo, X., Xiao, Z., Ling, L., 2014. Biosens. Bioelectron. 59, 54–57.

Nielsen, P.E., Egholm, M., Berg, R.H., Buchardt, O., 1991. Science 254, 1497–1500.

Nonin, S., Leroy, J.L., Gueron, M., 1995. Biochemistry 34, 10652−10659.

Nielsen, P.E., 2010. Curr. Opin. Mol. Ther. 12, 184–191.

Noorbakhsh, A., Salimi, A., 2011. Biosens. Bioelectron. 30, 188–196.

Ozkan, D., Erdem, A., Kara, P., Kerman, K., Gooding, J.J., Nielsen, P.E., Ozsoz, M., 2002. Electrochem. Commun. 4, 796–802.

Pintauer, T., Reinöhl, U., Feth, M., Bertagnolli, H., Matyjaszewski, K., 2003. Eur. J. Inorg. Chem. 2003, 2082−2094.

Pellestor, F., Paulasova, P., Hamamah, S., 2008. Curr. Pharm. Des. 14, 2439–2444.

Patterson, A., Caprio, F., Vallée-Bélisle, A., Moscone, D., Plaxco, K.W., Palleschi, G., Ricci, F., 2010. Anal. Chem. 82, 9109−9115.

Strobel, S.A., Dervan, P.B., 1991. Nature 350, 172–174.

Smolina, I.V., Demidov, V.V., Soldatenkov, V.A., Chasovskikh, S.G., Frank-Kamenetskii, M.D., 2005. Nucleic Acids Res. 33, e146–e146.

Schwarzenbach, H., Hoon, D.S., Pantel, K., 2011. Nat. Rev. Cancer 11, 426−437.

Stadler, A.L., Sun, D., Maye, M.M., van der Lelie, D., Gang, O., 2011. ACS Nano 5, 2467−2474.

Thuong, N.T., Hélène, C., 1993. Angew. Chem. Int. Ed. 32, 666−690.

Voloshin, O.N., Wang, L., Camerini-Otero, R.D., 1996. Science 272, 868–872.

Wu, C., Zhou, Y., Miao, X., Ling, L., 2011. Analyst 136, 2106−2110.

Wu, Y., Xue, P., Hui, K.M., Kang, Y., 2014. Biosens. Bioelectron. 52, 180−187.

Xiao, Z., Guo, X., Ling, L., 2013. Chem. Commun. 49, 3573−3575.

Zhu, H., Zhang, M., Zou, L., Li, R., Ling, L., 2017. Talanta 173, 9−13.

Figure captions:

Scheme 1. Schematic illustration of the electrochemical detection of dsDNA.

Fig. 1. (A) Native-PAGE assay. Lane 1 shows 20 pmol of dsDNA-T, lane 2 shows the mixture of 20 pmol PNA and 20 pmol dsDNA-T1, lane 3 shows the mixture of 20 pmol PNA and 40 pmol dsDNA-T. (B) SWV response of the PNA/MCH/dsDNA-T1/Zr^{4+}/BPAA/FMMA-modified electrode (a), and of that obtained without adding PNA (b), dsDNA-T (c), Zr^{4+} (d) BPAA (e), $Cu^{II}Br/L$ (f), or FMMA (g) during the sequential modification of the electrode. The supporting electrolyte was 0.5 M $LiClO_4$. For SWV measurements, the increase potential was 4.0 mV s^{-1}, the potential amplitude was 25 mV, and the quiet time was 30 s. (C) CVs of the PNA/MCH/dsDNA-T1/Zr^{4+}/BPAA/FMMA-modified electrode in 0.5 M $LiClO_4$ at the scan rates of 10, 25, 50, 75, 100, 150, 250, 500, 750 and 1000 mV s^{-1}. Inset: The linear relationship between oxidation (black line) and reduction (red line) peak currents and scan rate. (D) The Nyquist plots of EIS of the bare gold electrode (a), and of the (b) PNA-, (c) PNA/MCH-, (d) PNA/MCH/dsDNA-T1, (e) PNA/MCH/dsDNA-T1/Zr^{4+}-, (f) PNA/MCH/dsDNA-T1/Zr^{4+}/BPAA-, or (g) PNA/MCH/dsDNA-T1/Zr^{4+}/BPAA/FMMA-modified gold electrode in 0.1 M KNO_3 containing 5.0 mM $[Fe(CN)_6]^{3-/4-}$ as the redox probes. The concentration of dsDNA-T used for all electrochemical experiments was 1.0 nM. The eATRP time was 60 min.

Fig. 2. (A) SWV responses toward different concentrations of dsDNA-T over the range of 1.0 fM to 1.0 nM. (B) The calibration plot between the oxidation current at ~0.3 V (*vs.* SCE) and the logarithm of dsDNA-T concentration. The supporting electrolyte was 0.5 M $LiClO_4$. The experimental details for SWV measurements can be referred to Fig. 1B. Error bars represent the standard deviations of six independent experiments.

Fig. 3. (A) SWV responses at ~0.3 V (*vs.* SCE) toward different dsDNAs (1.0 nM, 10 μL). (B) SWV responses at ~0.3 V (*vs.* SCE) in the absence or presence of 10% normal human serum. The supporting electrolyte was 0.5 M $LiClO_4$. The experimental details for SWV measurements can be referred to Fig. 1B. Error bars represent the standard deviations of six independent experiments.

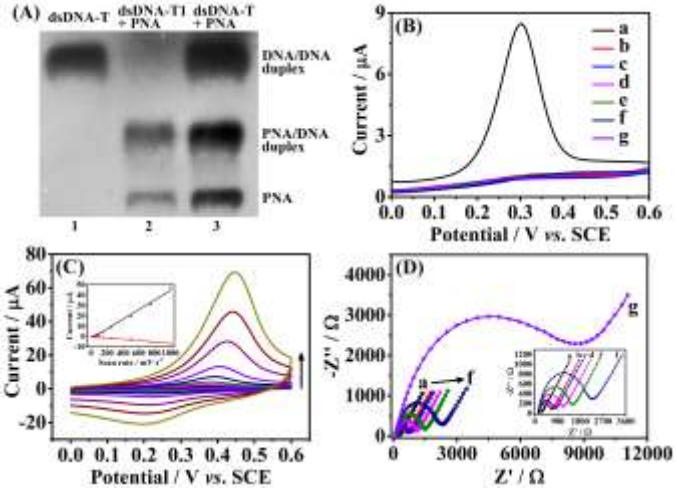
(A)
dsDNA-T
dsDNA-T1 + PNA
dsDNA-T + PNA
DNA/DNA duplex
PNA/DNA duplex
PNA
1
2
3
(B)
a
b
c
d
e
f
g
Current / μA
Potential / V vs. SCE
(C)
Current / μA
Potential / V vs. SCE
(D)
-Z'' / Ω
Z' / Ω

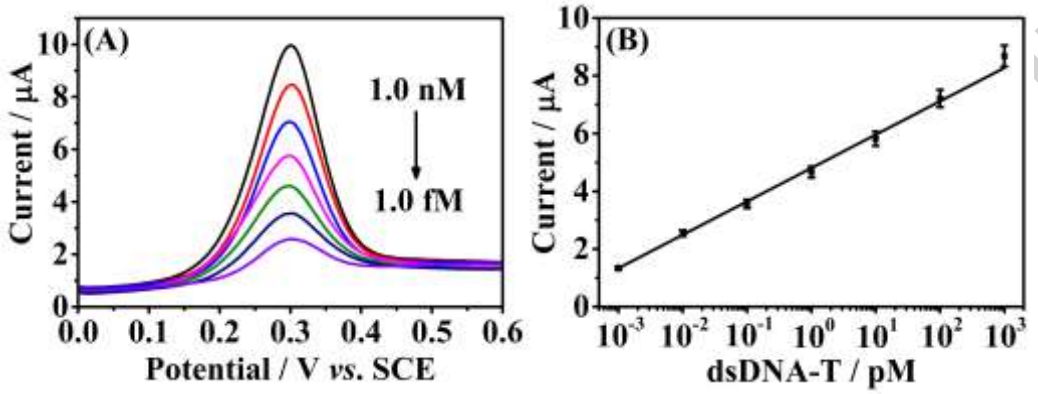
(A)
1.0 nM
1.0 fM
Current / μA
Potential / V vs. SCE
(B)
Current / μA
dsDNA-T / pM

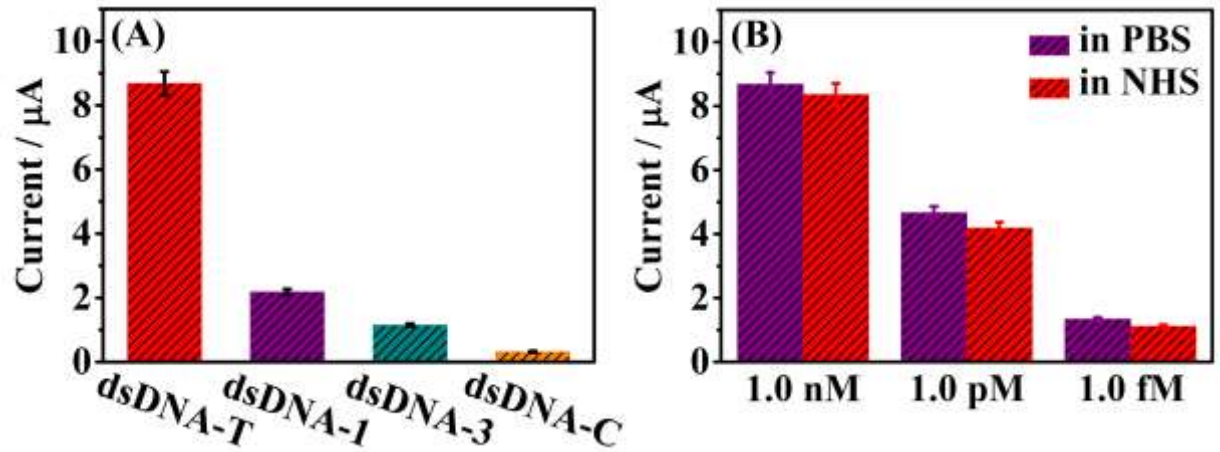
(A)
Current / μA
dsDNA-T
dsDNA-1
dsDNA-3
dsDNA-C
(B)
in PBS
in NHS
Current / μA
1.0 nM
1.0 pM
1.0 fM

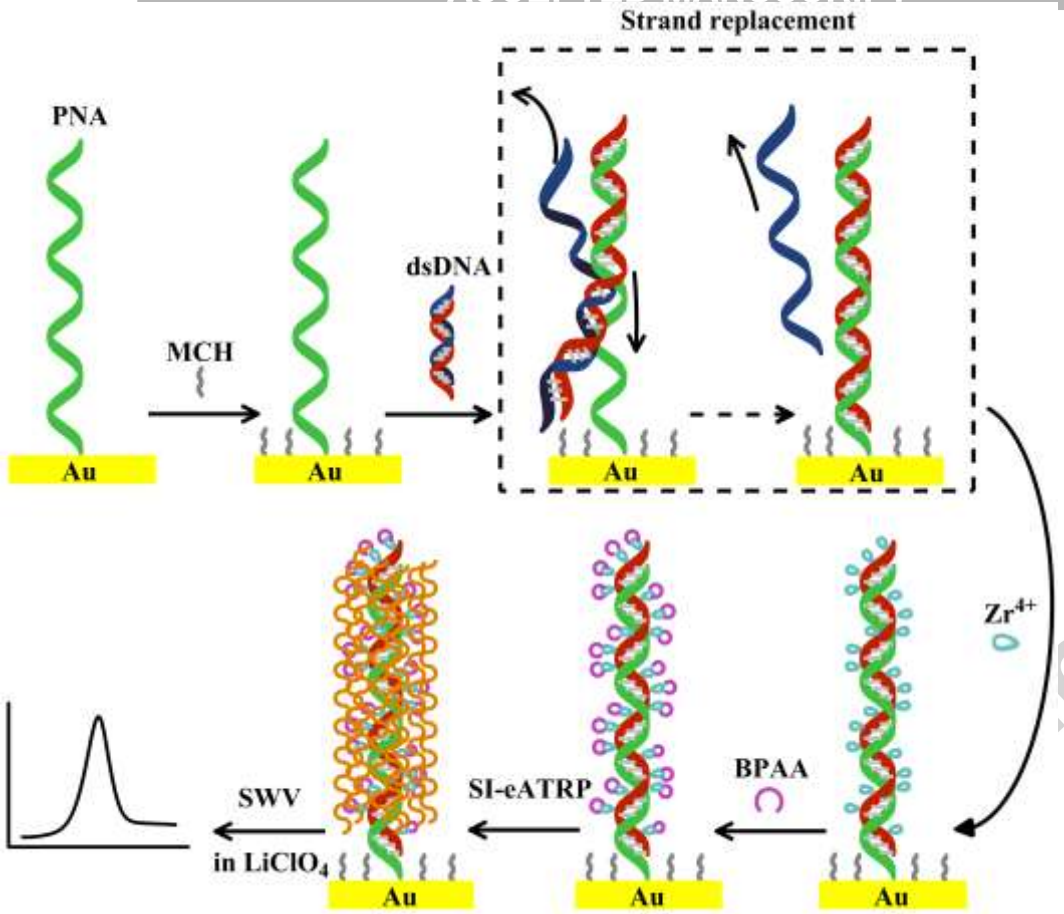

Table 1. Sequences of PNA and dsDNAs

Name	Sequence
PNA	5’-HS-$(CH_2)_{11}$-AAC CAT ACA ACC TAC TAC CTC A-3’
dsDNA-T	5’-TGA GGT AGT AGG TTG TAT GGT T-3’ (1) 3’-ACT CCA TCA TCC AAC ATA CCA A-5’ (2)
dsDNA-1	5’-TGA GGT AGT AGG TTG TGT GGT T-3’ (1) 3’-ACT CCA TCA TCC AAC ACA CCA A-5’ (2)
dsDNA-3	5’-TGA GGT ATT AGA TTG TGT GGT T-3’ (1) 3’-ACT CCA TAA TCT AAC ACA CCA A-5’ (2)
dsDNA-C	5’-ACT TAC CTT TGC TCA TTG ACG A-3’ (1) 3’-TGA ATG GAA ACG AGT AAC TGC T-5’ (2)

Table 2. Comparison of the analytical performance of our method with others

Method	Probe	Signal amplification	Linear range (nM)	LOD	Mode	Refs.
Fluorometric	PNA	No	0−2.0	0.26 nM	Signal-on	Lee et al., 2014
Electrochemical	TFO	HCR*+ AuNPs*	0.015−1.0	2.6 pM	Signal-on	Li et al., 2015
Colorimetric	TFO	HCR+ DNAzyme*	5.0×10^{-4}−0.5	0.1 pM	Signal-on	Li et al., 2017
Electrochemical	TFO	No	0.35−25	0.275 nM	Signal-off	Miao et al., 2014
Fluorometric	TFO	No	40−260	14.3 nM	Signal-on	Wu et al., 2011
Fluorometric	TFO	No	0.75−50	0.693 nM	Signal-on	Xiao et al., 2013
Fluorometric	TFO	Nicking enzyme	0.1−200	65 pM	Signal-on	Zhu et al., 2017
Electrochemical	PNA	SI-eATRP	10^{-6}−1.0	0.47 fM	Signal-on	This work

*HCR: hybridization chain reaction, AuNPs: gold nanoparticles, DNAzyme: asymmetrically split G-Quadruplex DNAzyme.

Highlights

(1) An electrochemical method is reported for the direct detection of dsDNA;

(2) Strand replacement of dsDNA by PNA enables the direct detection of mixed-base dsDNA;

(3) The high sensitivity can be ascribed to the electrochemically mediated polymerization;

(4) It is highly selective and reproducible, and holds high anti-interference capability;

(5) It provides a universal and efficient solution for the direct detection of dsDNA.